UDC 551.501.771:551.571.7:551.521.32:551.507.362.2 SIRS-B

Statistical Estimation of Precipitable Water With SIRS–B Water Vapor Radiation Measurements

WILLIAM C. SHEN—*Research Division, Control Data Corporation, Minneapolis, Minn.*

WILLIAM L. SMITH—*National Environmental Satellite Service, NOAA, Hillcrest Heights, Md.*

ABSTRACT—A multiple-parameter model has been formulated to estimate precipitable water profiles above the standard pressure levels from the satellite infrared spectrometer B (SIRS–B) radiation observations taken from the Nimbus 4 satellite. The method was verified with coincident radiosonde data. The relative error of SIRS-derived precipitable water above the 1000-mb level was approximately 20 percent. The 532-cm^{-1} water vapor channel alone explained 72 percent of the variance of the precipitable water. This method was used to specify the optimum SIRS–B spectral intervals for future water vapor sounding.

1. INTRODUCTION

The launch of the Nimbus 3 satellite in 1969 introduced a new era in the application of satellites to meteorological observations. The satellite infrared spectrometer (SIRS) provided highly accurate measurements that have been used to derive temperature and geopotential height profiles for routine operational use. For the Nimbus 4 satellite, six channels in the water vapor rotation band (referred to here as channels 1–6) were added to the SIRS instrument to provide measurements for estimating the vertical water vapor profile. Future Nimbus E infrared temperature profile radiometer (ITPR) and ITOS vertical temperature profile radiometer (VTPR) instruments will employ a single water vapor channel for specification of the total precipitable water.

With measurements in one spectral water vapor channel only, it is in principle not possible to give a more detailed picture of the vertical water vapor distribution than the mean value for a single, deep layer in the atmosphere. However, we will show that the characteristics of the precipitable water profile are highly correlated with the saturated precipitable water given by the temperature profile. As a result, some charateristics of the precipitable water profile may be inferred from water vapor radiances and the temperature profile using statistical relationships. The purposes of this study are (1) to determine the degree of accuracy to which the precipitable water vapor profiles in the troposphere can be specified from multichannel water vapor channel radiances as well as those observed by a single channel, given the temperature profile, and (2) to estimate optimum spectral intervals among the set measured by SIRS–B for obtaining the total precipitable water from future radiometric sounders.

A stepwise regression technique is used to determine the relationships between the total precipitable water above each mandatory pressure level considered and various independent parameters. The regression equations are based upon radiances computed for the various SIRS–B spectral intervals from radiosonde data to avoid cloud contamination. The regressions are then applied to actual SIRS radiance observations. The inferred water vapor profiles are verified with corresponding radiosonde data.

2. STATISTICAL MODEL

With the assumption of local thermodynamical equilibrium and no scattering by air molecules, the spectral radiance, N, upwelling from an atmosphere at the wave number ν, may be expressed as

$$N=B_\nu(p_s)\tau_\nu(p_s)-\int_0^{p_s} B_\nu(p)\,\frac{\partial \tau_\nu[U(p)]}{\partial p}\,dp \qquad (1)$$

where $B_\nu(p)$ is the Planck function at wave number ν and pressure level p, $\tau_\nu[U(p)]$ is the transmission function at wave number ν, U is the water vapor mass above the pressure level p, and subscript s denotes the surface condition. We assume in eq (1) that the surface has unit emissivity. The first term is the contribution from the surface, ground or cloud, and the second term denotes atmospheric contribution, which can be regarded as a weighted vertical average of the source function with a weighting function given by $\partial\tau_\nu[U(p)]/\partial p$. The SIRS–B water vapor channel weighting functions for a mean water vapor concentration are illustrated in figure 1.

The information content of radiation measurements has been studied previously by Twomey (1965), Mateer (1965), Rodgers (1966), Westwater and Strand (1968), and Fleming and Smith (1973). These studies have shown that the information obtainable from the inverse of the radiative transfer equation is limited by the interdepend-

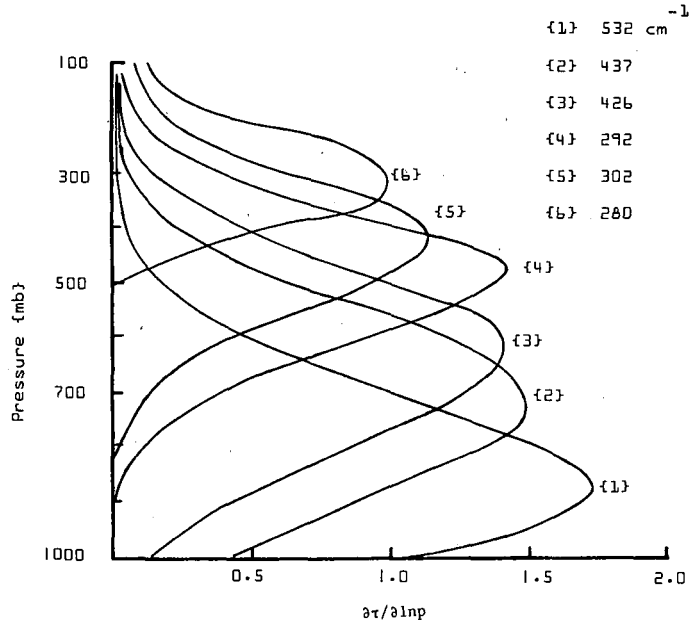

FIGURE 1.—Weighting functions ($\partial\tau/\partial \ln p$) for the Nimbus 4 SIRS–B water vapor channels.

ence of the measurements themselves. It is desirable to incorporate the statistical information that is well known from the standard measurements into satellite measurements for temperature and water vapor retrieval. This a priori knowledge is available and can be used to assess the usefulness of radiation measurements in the statistical specification of the unknown profiles.

In the early versions, a priori statistical information was utilized in the form of an orthogonal basis (Wark and Fleming 1966, Alishouse et al. 1967). The usual bases chosen were the eigenvectors arranged in decreasing order of eigenvalues. Strand and Westwater (1968) showed that a priori statistical information can be incorporated into the inversion algorithm in terms of standard covariance matrices. Conrath et al. (1970) suggested that a priori statistical information on precipitable water can be embodied in a set of linear regression equations relating the water vapor parameters to the satellite measurements.

Specification of Variables

In this study, the precipitable water above each pressure level, p, is expressed by an equation of the form

$$\ln U(p)=A_0+A_1X_1+A_2X_2+A_3X_3+\ldots+A_nX_n \quad (2)$$

where A_n are the regression coefficients, X_n are the independent variables, which are prespecified predictors, and n is the number of variables. A total of 30 variables was investigated. The logarithm of precipitable water has been previously shown by Smith and Howell (1971) to be linearly related to water vapor radiances.

The independent variables were chosen because of their physical relation with the precipitable water and can be either observed or inferred from satellite radiation measurements. They are listed in table 1. The variables considered in the computations are defined as:

1. The saturated precipitable water is defined by

$$U_s(p)=\frac{1}{g}\int_0^p w_s(p)dp \quad (3)$$

where g is the gravitational acceleration and $w_s(p)$ is the saturated mixing ratio, which can be specified from temperature only. The saturated precipitable water is the theoretical limit of the actual precipitable water and can be calculated from the satellite-derived temperature profiles. For our regression equation development, however, $U_s(p)$ was determined from the radiosonde temperatures.

2. Radiance difference ratios, Q_i, were used to limit the range of variability of the radiance predictors. The Q_i are given by

$$Q_i=\frac{N_i-N_{40,i}}{N_{40,i}} \quad (4)$$

where N_i is the radiance at wave number i and $N_{40,i}$ is the radiance at wave number i assuming 40 percent relative humidity. The radiances were computed for the six SIRS–B water vapor absorption channels using eq (1) with radiosonde data. These six ratios corresponding to the six water vapor channels were considered as the independent variables.

3. In the radiative transfer equation, the spectral radiance can be related to the precipitable water for a given temperature profile. The radiances computed from the radiosonde data, expressed in terms of equivalent blackbody temperatures, were also chosen as independent variables. These temperatures are weighted mean temperatures over a considerable layer of the atmosphere, each channel representing a different layer.

4. Temperatures at the mandatory pressure levels were also considered as independent variables, since they, as well as water vapor, determine the outgoing radiance measured in the SIRS–B water vapor channel.

Stepwise Regression

The stepwise regression procedure is an improved version of the forward-selection procedure. The improvements involve the reexamination at each step of the variables incorporated into the model in previous steps. Any variable that provides an insignificant contribution to the explained variances is removed from the analysis. The theoretical considerations for the stepwise regression and screening technique were discussed by Miller (1962). The numerical procedure of Efroymson (1962) has proven useful in practice and was used in this computer program.

All variables in table 1 were examined through regression screening. The order of selection of variable and the additional and cumulative explained variances of each variable are shown in table 1. The variance is not listed when the addition of the explained variance of $\ln U(p)$

TABLE 1.—*Explained variances of ln U (6 channels, 30 independent variables). Column 1 is the order of selection of variable, column 2 is the additional explained variance, and column 3 is the cumulative explained variance.*

Variable	Symbol	1000 mb			850 mb			700 mb			500 mb			300 mb			200 mb		
		(1)	(2)	(3)	(1)	(2)	(3)	(1)	(2)	(3)	(1)	(2)	(3)	(1)	(2)	(3)	(1)	(2)	(3)
1. Log of saturated precipitable water	$\ln(U_s)$	X_1	84.94	84.94	X_1	74.75	74.75	X_1	65.37	65.37	X_1	60.03	60.03	X_1	70.43	70.43	X_1	75.25	75.25
2. Saturated precipitable water (g·cm^{-2})	U_s	X_7	0.54	97.97															
3. Square of saturated precipitable water	U_s^2																		
4. Log of temperature	$\ln(T)$	X_6	0.25	97.43															
5. Temperature (°K)	T																		
6. Square of temperature	T^2				X_4	0.42	92.27	X_7	0.19	89.34							X_2	2.12	77.37
7. Radiance difference ratio	Q_1	X_2	8.78	93.72	X_2	9.93	84.68	X_3	3.64	86.14							X_7	0.43	80.70
8. Square of radiance difference ratio	Q_1^2	X_4	1.00	96.94	X_5	0.42	92.69												
9. Effective blackbody temperature (532 cm^{-1})	T_1				X_9	0.32	93.65	X_4	2.24	88.38							X_6	0.56	80.27
10. Square of effective blackbody temperature	T_1^2				X_{10}	0.28	93.93										X_4	0.43	79.01
11. Radiance difference ratio	Q_2				X_7	0.21	93.14												
12. Square of radiance difference ratio	Q_2^2				X_6	0.24	92.93										X_{10}	0.22	81.50
13. Effective blackbody temperature (437 cm^{-1})	T_2	X_3	2.22	95.94							X_3	1.46	88.13						
14. Square of effective blackbody temperature	T_2^2	X_8	0.44	98.41										X_3	1.22	80.72			
15. Radiance difference ratio	Q_3				X_8	0.19	93.33												
16. Square of radiance difference ratio	Q_3^2	X_5	0.24	97.18															
17. Effective blackbody temperature (426 cm^{-1})	T_3				X_3	7.17	91.85	X_{10}	0.31	90.24									
18. Square of effective blackbody temperature	T_3^2							X_2	17.13	82.50									
19. Radiance difference ratio	Q_4							X_6	0.36	89.15									
20. Square of radiance difference ratio	Q_4^2																		
21. Effective blackbody temperature (292 cm^{-1})	T_4										X_5	1.24	90.11						
22. Square of effective blackbody temperature	T_4^2										X_2	26.64	86.67						
23. Radiance difference ratio	Q_5																X_9	0.38	81.28
24. Square of radiance difference ratio	Q_5^2							X_5	0.41	88.79	X_4	0.74	88.87						
25. Effective blackbody temperature (302 cm^{-1})	T_5							X_9	0.49	89.93									
26. Square of effective blackbody temperature	T_5^2							X_8	0.10	89.44							X_8	0.20	80.90
27. Radiance difference ratio	Q_6													X_6	0.44	82.00			
28. Square of radiance difference ratio	Q_6^2										X_9	0.20	90.31	X_5	0.26	81.56	X_3	1.21	78.58
29. Effective blackbody temperature (280 cm^{-1})	T_6													X_2	9.07	79.50	X_5	0.70	79.71
30. Square of effective blackbody temperature	T_6^2													X_4	0.58	81.30			

is less than 0.1 percent. In arriving at the screened-version equations for one and six water vapor channels, we employed the discriminant technique based upon the analysis of the sequential F-test.

The basic data used in this study were radiosonde data and SIRS–B water vapor channel radiances. Northern Hemisphere radiosonde data were extracted from the National Meteorological Center (NMC) upper air automatic data processing magnetic tapes for three periods. Two periods (July 1–12, 1966, and Jan. 5–11, 1966) of 914 soundings were used to calculate moisture parameters and water vapor radiances used in the regression screening procedure. One period (June 1–8, 1970) of 68 soundings was used to verify the regression equation by comparing the radiosonde-derived precipitable water to the precipitable water derived from actual SIRS–B radiance measurements.

The moisture parameters calculated were vapor pressure, e, mixing ratio, q, total precipitable water, U, and relative humidity, r. The radiances corresponding to the six water vapor channels on SIRS–B were determined by eq (1) using absorption coefficients empirically determined by Smith and Howell (1971).

The reduction of variance afforded by three specifiers ($\ln U_s$, Q_i, and Q_i^2) with different combinations of water vapor channels are shown in table 2. The regression equations for predicting the precipitable water from the measured water vapor channel radiances have the form

$$U(p)=U_s^a(p)\,\exp\left[B_{0,n}(p)+\sum_{i=1}^{n}B_{1,i}(p)Q_i+\sum_{i=1}^{n}B_{2,i}(p)Q_i^2\right] \tag{5}$$

TABLE 2.—*Explained variances of ln U (1 channel, 2 channels, and 6 channels) based on 3 variables (ln U_s, Q_i, and Q)*†

	1 channel						2 channels	
	(1) 532 cm^{-1}	(2) 437 cm^{-1}	(3) 426 cm^{-1}	(4) 292 cm^{-1}	(5) 302 cm^{-1}	(6) 280 cm^{-1}	(1)+(4)	6 channels
200 mb	75.30	75.26-	75.29	76.35	76.68	77.01	76.35	77.01
300 mb	71.01	70.82	71.40	76.29	77.72	78.43	76.37	78.64
500 mb	63.10	61.79	69.52	83.92	84.31	77.98	84.20	84.81
700 mb	71.03	66.32	72.86	81.17	79.81	74.47	83.18	83.18
850 mb	85.43	75.58	76.83	81.86	81.23	78.88	88.69	88.88
1000 mb	95.13	86.27	85.33	87.73	87.51	86.57	95.13	95.13

where $n=1, 2, 3, \ldots, 6$ and α, $B_{0,n}(p)$, $B_{1,i}(p)$, and $B_{2,i}(p)$ are the regression coefficients. For use with measurements from a single water vapor channel, eq (5) reduces to

$$U(p)=U_s^{\alpha}(p)\exp\left[B_0(p)+B_1(p)Q+B_2(p)Q^2\right]. \qquad (6)$$

The coefficients (α, B_0, B_1, and B_2) of the regression equations for each of the six water vapor channels at six pressure levels are shown in figure 2.

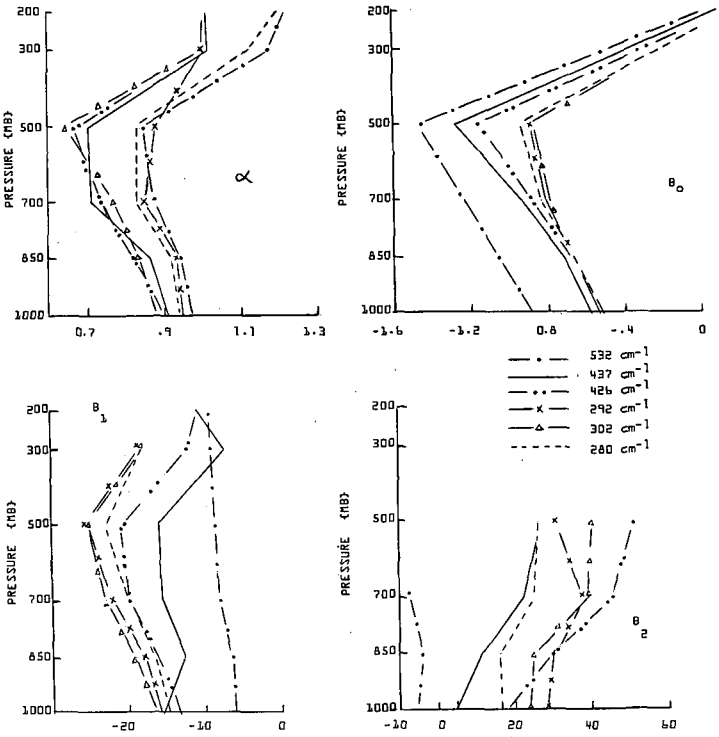

FIGURE 2.—Coefficients of the regression equations for each of the six water vapor spectral intervals of SIRS–B.

Regression Analysis of Precipitable Water Profile

The regression analysis of the precipitable water revealed several features concerning the specification of the logarithm of the precipitable water, ln U:

1. The reduction of variance of ln U above each mandatory level is mainly explained by two or three variables; they are, the logarithm of the saturated precipitable water, ln U_s, and variables defined from radiances of one or two water vapor channels. As would be expected, more variance of the logarithm of the precipitable water profile, ln U, is explained by using six channels than by any one channel separately. However, the optimum choice of two spectral intervals to specify the amount of precipitable water above each level was nearly as good as six spectral intervals because of the interdependence and correlation of the water vapor in the layers sensed by the six water vapor channels.

2. The explained variances show a definite height-dependent pattern. The 532-cm^{-1} and 437-cm^{-1} channels have higher information content in the lower troposphere where the moisture content is largest. The 426-cm^{-1} and 292-cm^{-1} channels furnished more information in the middle troposphere, while the 302-cm^{-1} and 280-cm^{-1} channels have more information available in the high troposphere.

3. The 532-cm^{-1} channel is a favorite single choice because of its ability to infer the precipitable water above the 1000-mb level most accurately. A channel more transparent to water vapor than the SIRS–B 532-cm^{-1} channel would be expected to give even better results.

3. ALGORITHM FOR WATER VAPOR ESTIMATES

An iterative method of solving the radiative transfer equation for the relative humidity, $r(p)$, from six water vapor radiances has been developed by Smith (1970). However, when only one spectral measurement is made (as in the case with the Nimbus E ITPR and ITOS D VTPR), a priori statistical information concerning the vertical structure of the water vapor mass distribution can be used in an iterative method to yield a more accurate solution for the vertical structure.

By differentiation of eq (5), we obtain

$$\delta U(p)=U(p)\left(\sum_{i=1}^{n}B_{1,i}+2\sum_{i=1}^{n}B_{2,i}Q_i\right)\frac{\delta N_i}{N_{40,i}}, \qquad i=1, 2, \ldots, . \qquad (7)$$

Substituting eq (7) into the standard iterative form,

$$U^{j+1}(p)=U^j(p)+\delta U^j(p), \qquad (8)$$

produces the following algebraic equation:

$$U^{j+1}(p)=U^j(p)\left[1+\sum_{i=1}^{n}\left(\frac{B_{1,i}+2B_{2,i}Q_i}{N_{40,i}}\right)\delta N_i^j\right]. \qquad (9)$$

From the precipitable water, other moisture parameters can be determined. The relative humidity, $r(p)$, is related to U by

$$r(p)=\frac{g(p-e_s)}{0.622e_s}\frac{\partial U(p)}{\partial p}\approx\frac{gp}{0.622e_s}\frac{\partial U(p)}{\partial p} \qquad (10)$$

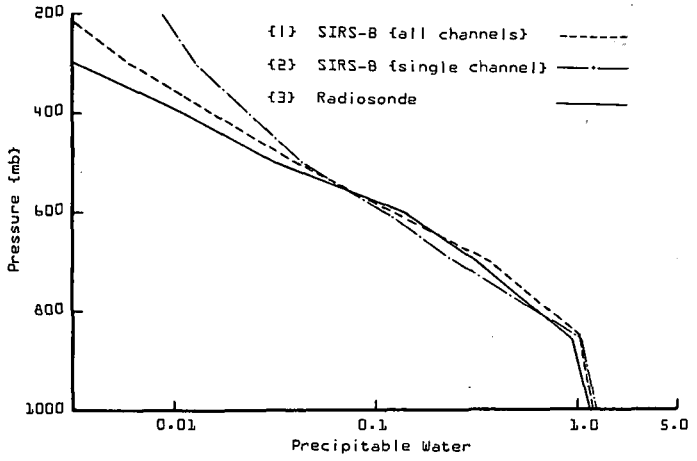

FIGURE 3.—Comparison of a middle latitude, SIRS–B derived precipitable water profile ($g \cdot cm^{-2}$) with a radiosonde sounding over Aughton, England, at 2300 GMT, June 4, 1970.

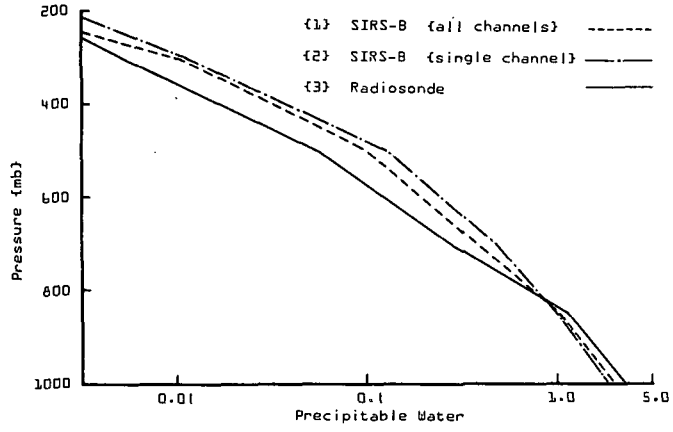

FIGURE 4.—Comparison of a low-latitude, SIRS–B derived precipitable water profile ($g \cdot cm^{-2}$) with a radiosonde sounding over Swan Island at 1200 GMT, June 1, 1970.

where e_s is the saturated vapor pressure, g is the gravitational acceleration, and p is the pressure. The mixing ratio $q(p)$ is given by

$$q(p)=g\frac{\partial U(p)}{\partial p}. \tag{11}$$

To begin the iterative precedure, we made an initial estimate of the precipitable water profile from eq (5). The radiance is computed using eq (1), with the given temperature and the estimated precipitable water profiles. The calculated and measured radiances are then used to compute a new estimate of the precipitable water profile using eq (9). The procedure is repeated until the root-mean-square (rms) difference between the calculated and the measured radiances is less than a predetermined value. Once the precipitable water profile has been calculated, the relative humidity profile is evaluated from eq (10).

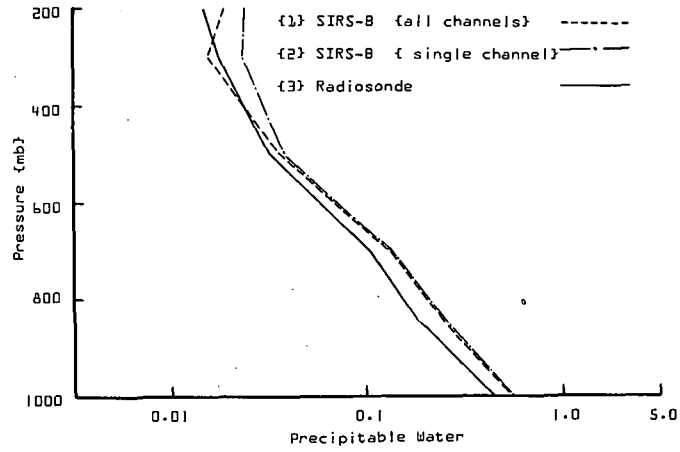

FIGURE 5.—Comparison of a high-latitude, SIRS–B computed precipitable water profile ($g \cdot cm^{-2}$) with a radiosonde sounding over Barrow, Alaska, at 1200 GMT, June 5, 1970.

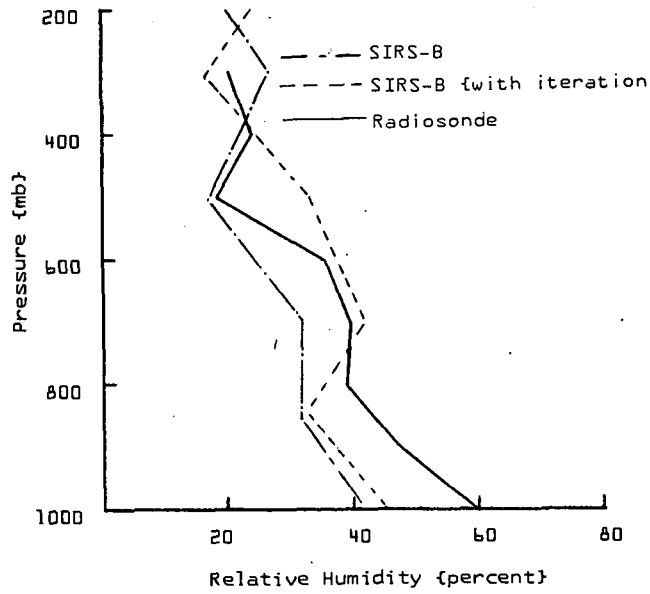

FIGURE 6.—Comparison of a SIRS–B derived relative humidity profile with a Stornoway, Scotland, sounding at 1200 GMT, June 4, 1970.

4. RESULTS

Comparison of SIRS–B Derived Precipitable Water Profiles

Comparison of the SIRS–B reconstructed precipitable water profiles found from eq (9) with corresponding radiosonde precipitable water profiles was made in figures 3–5. They were chosen to typify low-, middle-, and high-latitude profiles. The dashed line in figure 3 represents the SIRS–B all-channel precipitable water profiles, the dash-dotted line represents the SIRS–B single-channel (532 cm^{-1}) precipitable water profile, and the solid line represents the radiosonde precipitable water profile. The sounding was taken at Aughton, England (53.6°N, 2.9°W), at 2300 GMT on June 4, 1970. The Nimbus 4

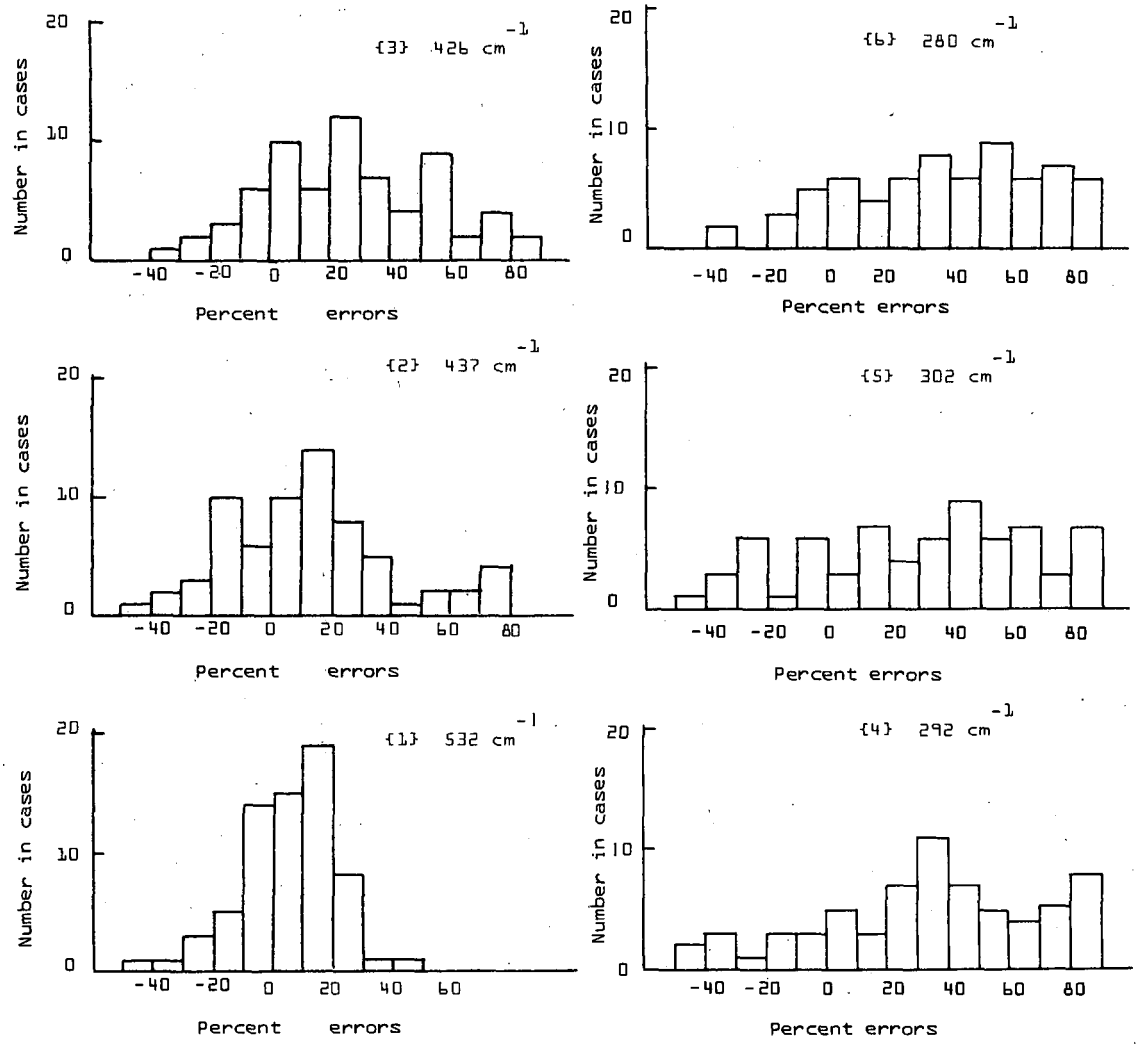

FIGURE 7.—Distribution of percent errors of SIRS–B derived total precipitable water for each of the six water vapor channels.

satellite passed over this station at 0019 GMT, resulting in a time lag of about 1 hr. The three profiles agree well, below the 500-mb level. The "all-channel" solution of the precipitable water in the upper troposphere is significantly better than the single-channel (532 cm^{-1}) solution.

Figure 4 shows a comparison of a typical tropical sounding. The radiosonde sounding was taken at Swan Island (17.4°N, 83.9°W) at 1200 GMT on June 1, 1970. The satellite passed over this station at 0621 GMT, giving a 6-hr time difference. The three profiles did not agree very well except near the 850-mb level. Large differences are apparent at the 1000-mb level and above the 700-mb level. The error of the derived total precipitable water above the 1000-mb level was about 1 $g \cdot cm^{-2}$ for both all-channel and single-channel solutions of the precipitable water.

Comparison of the three types of profiles in the Arctic region is given in figure 5. This case is typical of a high-latitude, summer sounding. The precipitable water at ground level is quite low, and it decreases slowly with height. The radiosonde was taken at Barrow, Alaska (71.3°N, 156.8°W), at 1200 GMT on June 5, 1970. The Nimbus 4 satellite passed over this station at 1343 GMT. The three profiles compare well.

The SIRS–B relative humidity profiles reconstructed from Nimbus 4 SIRS–B radiance data are shown in figure 6. The sounding was taken at Stornoway, Scotland (58.2°N, 6.3°W), at 1100 GMT on June 4, 1970. The Nimbus 4 satellite passed over this station at 1042 GMT. It is interesting to compare solutions of the relative humidity obtained without iteration with those obtained through iteration. The dashed curve represents the SIRS–B relative humidity profile obtained through iteration, the dash-dotted curve represents those obtained without iteration, and the solid curve represents the radiosonde relative humidity profile. The three profiles agree quite well, never departing more than 20 percent at any pressure level. However, the relative humidity profile obtained through iteration was predicted more accurately in the lower troposphere than that reconstructed without iteration.

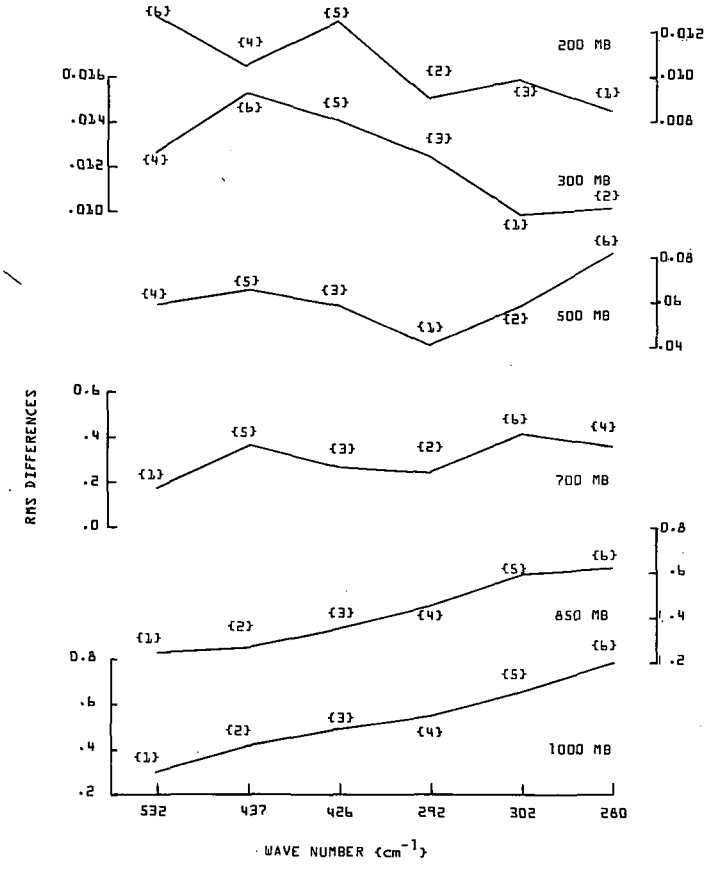

FIGURE 8.—Single-channel rms differences of SIRS–B precipitable water (g·cm^{-2}) at six pressure levels. Value in the parentheses is the ranking according to minimum difference.

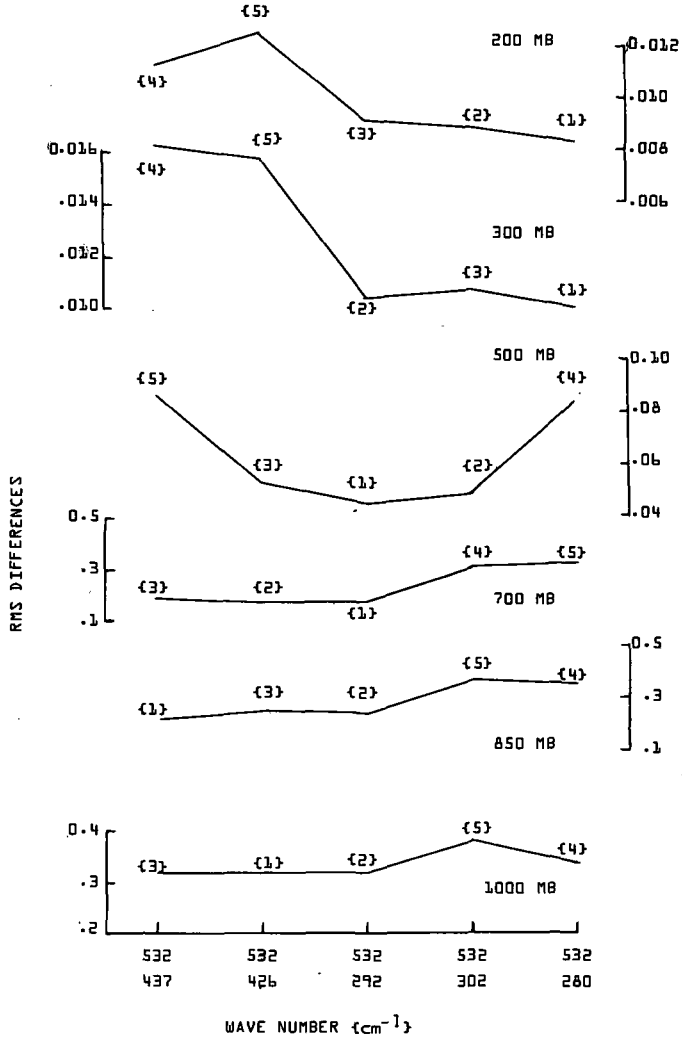

FIGURE 9.—Same as figure 8 for two-channel rms differences.

Distribution of Errors Resulting From the Regression Equation

The parameter S_u, defined as

$$S_u = \frac{U_{\text{recon}} - U_{\text{true}}}{U_{\text{true}}},$$

was computed for 68 cases. Here, S_u represents the percent error of the total precipitable water above the 1000-mb level. Figure 7 shows a histogram for the total precipitable water reconstructed from the radiance data of the six water vapor channels. Note that there is a tendency for error classes to shift toward more extreme values in the positive sense as the spectral intervals become more opaque. However, the distribution of percentage error for the 532-cm^{-1} channel is quite uniform about the mean error and has only small variance. Furthermore, the 532-cm^{-1} channel showed the smallest mean percentage error, 20 percent.

Information Content

The stepwise regression equations for computing precipitable water were used to determine how well the precipitable water calculated from radiosondes agrees with that calculated from the radiances measured in various channels of SIRS. Data consisting of 68 sets of SIRS–B radiances and matching radiosonde data were chosen for the test. The calculated precipitable water was compared with the observed precipitable water, level by level, from the 1000- to 200-mb levels. The rms differences indicate the specification accuracy and reveal that part of the atmosphere best sensed by the various SIRS channels. Using the rms difference as a measure of the information content of the water vapor radiation, one can define an optimum set of measurements as that set with minimum rms errors.

Figure 8 shows the distribution of rms differences of the SIRS-derived precipitable water above the mandatory pressure levels, resulting from the use of single-channel water vapor radiance measurements. The rankings of the six water vapor channels for a one-channel optimum are also shown in the figure. It can be seen that the rms difference of the reconstructed precipitable water of the 532-cm^{-1} water vapor channel is the smallest in the lower troposphere, where the largest moisture gradient exists.

TABLE 3.—*Multiple-channel rms differences of SIRS–B derived precipitable water profile* ($g \cdot cm^{-2}$)

	1-channel (1)	2-channel (1, 4)	3-channel (1, 4, 6)	4-channel (1, 3, 4, 6)	6-channel (1–6)
200 mb	0. 0128	0. 0092	0. 0086	0. 0086	0. 0099
300 mb	. 0127	. 0104	. 0103	. 0103	. 0166
500 mb	. 0594	. 0452	. 0450	. 0445	. 0641
700 mb	. 172	. 165	. 165	. 160	. 162
850 mb	. 244	. 245	. 245	. 245	. 243
1000 mb	. 309	. 309	. 309	. 309	. 307
Fractional variance reduction (percent)	72	81	82. 4	83. 1	72

As expected, the rankings of the six water vapor channels show a height-dependent pattern. The channels of 532, 437, and 425 cm^{-1} have higher information content below the 600-mb level in the lower troposphere. The variables from channels 292, 302, and 280 cm^{-1} furnish more information above the 600-mb level in the upper troposphere.

Figure 9 shows the two-channel rms differences of the SIRS–B derived precipitable water above the mandatory levels, resulting from the information added by two-channel radiance measurements. The rankings are also given in the figure. Since the 532-cm^{-1} channel, which is the 1-channel optimum, is the best choice in the lower troposphere for estimating precipitable water, two-channel rms errors were computed for the combination of the 532-cm^{-1} channel with other channels. An examination of the values of the average ranking suggested that a two-channel optimum is a combination of the 532- and 292-cm^{-1} channels.

The stepwise regression of the precipitable water, based on radiances from the six water vapor channels, showed the following:

1. The three-channel optimum set consists of channels 1, 4, and 6 (532 cm^{-1}, 292 cm^{-1}, and 280 cm^{-1}).

2. The four-channel optimum set consists of channels 1, 3, 4, and 6 (532 cm^{-1}, 426 cm^{-1}, 292 cm^{-1}, and 280 cm^{-1}).

The computed rms differences are given in table 3. Note that, as each of the channels was successively added, the rms differences decreased, especially above 700 mb. The last column in table 3 shows the rms differences of SIRS–B derived precipitable water based on six-channel radiance data. An examination of the values suggests that rms differences are larger for six channels than that for four channels. This is contrary to what one would expect and to the finding in the regression analysis. Because the regression equations were derived from simulated data using radiosondes, errors of measurement and incorrect transmission data (possibly for channel 5) may explain this discrepancy. The fractional variance reduction is 72 percent for the 532 cm^{-1} channel alone, 81 percent for the two-channel optimum, 82.4 percent for the three-channel optimum, and 83.1 percent for the four-channel optimum. Although each successive measurement reduces the variance, the reduction of variance after the first two measurements are added is small.

Analysis of Reconstruction Error

Many factors contribute to errors in the reconstruction of the precipitable water profiles. The factors are:

1. Errors are introduced when a high, thin cirrus or aerosol contaminates the radiances. The error in reconstructing the precipitable water profile will be determined by the radiance error. In a simulation experiment using a sounding at Chanwell, England (56.4°N, 2.9°W), on June 7, 1970, a 10-percent error in radiance caused a 28-percent error increase in the derived precipitable water above the 1000-mb level.

2. Uncertainty of the transmission function used in the radiative transfer equation could contribute errors in the computation.

3. Measurement errors in radiosonde temperature and dewpoint temperature could also contribute to the errors in the regression equation.

4. Time and space differences between the observations of radiosonde and radiation data could cause errors.

5. SUMMARY AND CONCLUSION

To improve the specification of the precipitable water above each mandatory pressure level from satellite radiation data, we have formulated a multiple-parameter model for estimating precipitable water profiles. A stepwise regression technique was used to determine the relationship between precipitable water derived from radiosonde data and 30 possible variables derived from satellite observations. The regression equations used simulated SIRS–B radiances computed from radiosonde data to avoid cloud contamination. This set of regression equations was then tested on actual SIRS–B water vapor radiance data.

The results show that the SIRS–B precipitable water profiles derived by this model compare favorably with the radiosonde-observed precipitable water profiles. In the comparison of SIRS and radiosonde profiles, the average difference of the precipitable water above the 1000-mb level was approximately 20 percent.

Calculations were made of the information content for the troposphere of each of the six SIRS–B water vapor channel, radiance measurements. The best combinations of six possible channels, taken 1, 2, 3, or 4 at a time, were determined. This work can be used for selecting the optimum spectral intervals from among the set measured by SIRS–B; however, there are other spectral intervals that may also be useful in water vapor sounding. For example, intervals more transparent than that at 532 cm^{-1} could conceivably improve the retrievals in the lower atmospheric levels.

It can be concluded from this study that precipitable water profiles can be determined reasonably well from SIRS–B. Since this technique is simple to use and provides accurate results, it can be a useful operational tool.

ACKNOWLEDGMENTS

The authors wish to thank A. Belmont, H. Howell, D. Hovland, and G. Nicholas for their contributions to this study.

492-846 O - 73 - 5

REFERENCES

Alishouse, J. C., Crone, L. J., Fleming, H. E., Van Cleef, F. L., and Wark, D. Q., "A Discussion of Empirical Orthogonal Functions and Their Application to Vertical Temperature Profiles," *Tellus*, Vol. 19, No. 3, Stockholm, Sweden, **1967**, pp. 477–482.

Conrath, B. J., Hanel, R. A., Kunde, V. G., and Prabhakara, C., "The Infrared Interferometer Experiment on Nimbus 3," *Journal of Geophysical Research*, Vol. 75, No. 30, Oct. **1970**, pp. 5831–5857.

Efroymson, M. A., "Multiple Regression Analysis," *Mathematical Methods for Digital Computers*, A. Ralston and H. S. Wilf (Editors), John Wiley and Sons, Inc., New York, N.Y., **1962**, 293 pp. (See pp. 191–203.)

Fleming, H. E., and Smith, W. L., "Inversion Techniques for Remote Sensing of Atmospheric Temperature Profiles," *Proceedings of the Fifth Symposium on Temperature, Its Measurement and Control in Science and Industry*, June 21–24, 1971, National Bureau of Standards, Gaithersburg, Md., **1973** (in press).

Mateer, Carlton L., "On the Information Content of Umkehr Observations," *Journal of the Atmospheric Sciences*, Vol. 22, No. 4, July **1965**, pp. 370–381.

Miller, Robert G., "Statistical Prediction by Discriminant Analysis," *Meteorological Monographs*, American Meteorological Society, Vol. 4, No. 25, Boston, Mass., Oct. **1962**, 54 pp.

Rodgers, C. O., "Satellite Infrared Radiometer: A Discussion of Inversion Methods," *Memorandum* No. 66.13, University of Oxford, Clarendon Laboratory, England, Sept. **1966**, 25 pp.

Smith, W. L., "Iterative Solution of the Radiation Transfer Equation for Temperature and Absorbing Gas Profiles of an Atmosphere," *Applied Optics*, Vol. 9, No. 9, Sept. **1970**, pp. 1993–1999.

Smith, W. L., and Howell, H. B., "Vertical Distributions of Atmospheric Water Vapor from Satellite Infrared Spectrometer Measurements," *Journal of Applied Meteorology*, Vol. 10, No. 5, Oct. **1971**, pp. 1026–1034.

Strand, O. N., and Westwater, E. R., "Minimum-rms Estimation of the Numerical Solution of a Fredholm Integral Equation of the First Kind," *SIAM Journal of Numerical Analysis*, Vol. 5, No. 2, June **1968**, pp. 287–292.

Twomey, S., "The Application of Numerical Filtering to the Solution of Integral Equations Encountered in Indirect Sensing Measurements," *Journal of the Franklin Institute*, Vol. 279, No. 2, Feb. **1965**, pp. 95–109.

Wark, D. Q., and Fleming, H. E., "Indirect Measurements of Atmospheric Temperature Profiles From Satellites: I. Introduction," *Monthly Weather Review*, Vol. 94, No. 6, June **1966**, pp. 351–362.

Westwater, Ed R., and Strand, Otto Neall, "Statistical Information Content of Radiation Measurements used in Indirect Sensing," *Journal of the Atmospheric Sciences*, Vol. 25, No. 5, Sept. **1968**, pp. 750–758.

[*Received February 27, 1972; revised May 18, 1972*]